



Contents lists available at ScienceDirect

Comparative Biochemistry and Physiology - Part D: Genomics and Proteomics

journal homepage: www.elsevier.com/locate/cbpd

Comparative transcriptome elucidates key genes and pathways related to golden phenotype of *Crassostrea gigas*

Yue Min^{a,b}, Qi Li^{a,b,c,*}, Hong Yu^{a,b}, Lingfeng Kong^{a,b}, Shikai Liu^{a,b}^a Key Laboratory of Mariculture (Ocean University of China), Ministry of Education, Ocean University of China, Qingdao 266003, China^b College of Fisheries, Ocean University of China, Qingdao 266003, China^c Laboratory for Marine Fisheries Science and Food Production Processes, Qingdao National Laboratory for Marine Science and Technology, Qingdao 266237, China

ARTICLE INFO

Edited by Chris Martyniuk

Keywords:

Crassostrea gigas
Pheomelanin
Transcriptome analysis
Melanosomal pH

ABSTRACT

Marine bivalves are economically important and exhibit a remarkable diversity in shell color. The Pacific oyster *Crassostrea gigas* stands out as an important economic species, with the successful development of four distinct color strains through selective breeding. While previous studies have shed light on the genetic mechanism underlying color segregation, the precise molecular regulatory mechanisms responsible for shell coloration in oysters remains elusive. In this study, we confirmed that the golden phenotype is primarily attributed to pheomelanin by histological and ultrastructural observations. Additionally, we conducted a comparative transcriptome analysis of the black and golden shell color oysters to explore the potential genes and pathways contributing to the golden phenotype in *C. gigas*. Our results revealed a significant increase in differentially expressed genes in the golden phenotype associated with pathways such as glutathione metabolism, and calcium signaling pathway, suggesting a potential role in the synthesis of pheomelanin. Of particular note, we highlighted the potential role of two-pore channel 2 (TPC2) in modulating tyrosinase activity and melanosomal pH, ultimately determining the shade of pigmentation. Our study in this work provided a preliminary exploration of the mechanism, shedding light on the melanosome microenvironment and shell color.

1. Introduction

Color polymorphisms are ubiquitously distributed in the animal kingdom associated with various biological functions, including camouflage, thermoregulation, photoprotection, mimicry, or warning predators (Hubbard et al., 2010). Certain species serve as ideal models for studying the genetic mechanisms responsible for color phenotypes (Hubbard et al., 2010). Color traits have been widely considered as distinctive phenotypes for morphological selection and identification. In the aquaculture industry, pigmentation is a crucial quality criteria, influencing the market value of aquatic products for both consumption and ornamental purposes (Harpaz and Padowicz, 2007). In recent years, artificial breeding of bivalves has developed several new color strains, including golden, orange, and black phenotypes of oyster (Ge et al., 2015; Xu et al., 2017; Han and Li, 2020), red phenotype of scallop (Chen et al., 2020), Manila clam (Yue et al., 2015) and more. Crossing studies in bivalves have elucidated that shell coloration constitutes a heritable trait governed by a restricted number of genes exhibiting discernible patterns of dominance (Brake et al., 2004; Zheng et al., 2013). In

Crassostrea gigas, the orange color is recessive to black and white, while the golden color is dominant over the white color (Ge et al., 2015; Han and Li, 2020). In *Pinctada margaritifera*, the proposed model for shell trait is one-locus three-allele system without co-dominance. In this model, black dominates over red coloration, which, in turn, prevails over the white shell (Ky et al., 2016). Furthermore, multiple studies have documented that shell coloration in *Haliotis discus hannai* Ino (Kobayashi et al., 2004; Liu et al., 2009), *Macoma balthica* (Luttikhuisen and Drent, 2008), and *Hyriopsis cumingii* (Wen et al., 2013) involves multiple alleles at single locus. Some variations are governed by a second locus, exerting epistatic control over other colors, as observed in the orange shell coloration in *Chlamys nobilis* (Zheng et al., 2013) and the purple shell coloration in *Argopecten purpuratus* (Winkler et al., 2001). Additionally, certain color variations might be influenced by more than two loci, as exemplified by the orange shell in *Argopecten purpuratus* (Winkler et al., 2001). In addition to the fascinating diversity in shell coloration observed across bivalve species, the molecular intricacies behind these hues remain poorly understood.

Melanin is present in a broad variety of organisms, including fungi,

* Corresponding author at: Key Laboratory of Mariculture, Ministry of Education, Ocean University of China, Qingdao 266003, China.

E-mail address: qili66@ouc.edu.cn (Q. Li).

<https://doi.org/10.1016/j.cbpd.2024.101197>

Received 26 September 2023; Received in revised form 22 January 2024; Accepted 22 January 2024

Available online 26 January 2024

1744-117X/© 2024 Elsevier Inc. All rights reserved.

plants, and animals, and is divided into two categories: eumelanin (black and brown pigments) and pheomelanin (red and yellow pigments) (Sun et al., 2023). The ratio of eumelanin and pheomelanin determines the shade of color (Caro and Mallarino, 2020). Both types of melanin begin with the tyrosine by enzymatic and non-enzymatic process (Lai et al., 2018; Solano, 2018; Pavan and Sturm, 2019). Pheomelanin synthesis primarily relies on non-enzymatic reactions and is influenced by the levels of dopaquinone and cysteine (D'Alba and Shawkey, 2019). Additionally, the melanosome of weak acidic pH promotes the synthesis of pheomelanin (Wakamatsu et al., 2017).

Melanosomal pH is a crucial determinant of melanogenesis. Originating from lysosomes (Raposo and Marks, 2007), these organelles may potentially involve various lysosomal ion channels or transporters that contribute to maintaining cellular homeostasis by storing intracellular ions. Two-pore channel 2 (TPC2) is an example of known melanosomal channels. It is localized to the melanosomes, where it is gated by the phosphatidylinositol 3,5- bisphosphate (PI (3,5) P2) and plays roles in the control of melanosomal pH and membrane potential (Bellono et al., 2016). In particular, the loss function of TPC2 resulted in melanosomal alkalinization, promoting pigmentation, whereas the gain function of TPC2 led to melanosomal acidification, which hindered melanogenesis (Ambrosio et al., 2016; Bellono et al., 2016).

The Pacific oyster *C. gigas*, an economically important marine bivalve species with a wide distribution, exhibits a variety of shell colors. The colors are not only distinctive but also significantly influence consumers' taste thresholds, sweetness perception, food preference, pleasantness, and acceptability (Kang et al., 2013). In recent years, selective breeding has developed different shell color strains of *C. gigas*, including white, black, golden, and orange (Ge et al., 2015; Xu et al., 2019; Han and Li, 2020), showcasing distinct phenotypes that provide an opportunity to investigate specific pigmentation mechanisms. This study integrated transcriptomic data with phenotypic and functional assays to elucidate the molecular regulatory mechanism underlying the golden phenotype in the *C. gigas*.

2. Materials and methods

2.1. Sample collection

One-year-old black and golden shell strains Pacific oysters were collected from Laizhou, Shandong, China. Three individuals from each of the shell color strains were collected. Left edge mantles were dissected, flash-frozen in liquid nitrogen, and reserved at -80°C freezer until RNA extraction.

2.2. Mantle melanin granules observation

2.2.1. Light microscope observation

To compare the distribution of melanin between black and golden oysters, we utilized ferrous sulfate staining kit (Leagene, China) with minor adjustment to the manufacturer's protocols. Paraffin-embedded sections were prepared and treated with xylene and gradient ethanol (95 %, 80 %, 70 %, 50 %). Subsequently, the sections were sequentially stained with ferrous sulfate and acid potassium ferricyanide solutions, followed by rinsing with ultrapure water. For counterstaining, nuclear fast red solution was applied to the sections, and images were captured using an Olympus BX53 light microscope after washing.

2.2.2. Transmission electron microscope observation

The mantles of black and golden shell color oysters were cut into 1 mm^3 size and fixed into 2.5 % glutaraldehyde at 4°C . The fixed tissues were then washed with 0.1 M PBS (phosphate-buffered saline) and post-fixed in 1 % osmium tetroxide to preserve the cellular structure. Subsequently, the tissues were dehydrated with a series of ethanol washes and embedded in resin. Finally, ultra-thin sections (around 60 nm) were stained with heavy metal solutions and imaged using a JEM-1200EX

transmission electron microscope (JEOL, Japan).

2.3. Quantitation of eumelanin and pheomelanin

The double antibody sandwich method was applied to detect the content of eumelanin and pheomelanin level according to the manufacturer's protocol. Initially, microporous plates were special, with purified pheomelanin or eumelanin antibody coated to create a solid-phase antibody. Subsequently, the pheomelanin and eumelanin samples were added to the microporous plates and bound with the HRP-conjugated eumelanin/pheomelanin antibodies, forming an antibody-antigen-enzyme complex. After washing, the color reaction occurred with the substrate of TMB. TMB turned blue under the catalysis of the HRP enzyme, and was then converted to the final yellow color with the function of acid. The shade of color was positively correlated with the amount of the pheomelanin and eumelanin in the sample. Absorbance was measured at a wavelength of 450 nm, and the concentration of eumelanin or pheomelanin was determined using a standard curve.

2.4. Transcriptome sequencing analysis

2.4.1. RNA extraction

The collected edge mantle tissues were extracted using TRIZOL reagent (Invitrogen) according to the manufacturer's instructions. RNA integrity and contamination were detected on 1 % agarose gels. RNA purity was checked using the Nanophotometer® spectrophotometer (Implen, GER). Qubit RNA Assay Kit in Qubit® 2.0 Fluorometer (Life technologies, CA, USA) was used to measure RNA concentration. RNA Integrity Number (RIN) was evaluated using the RNA Nano 6000 Assay Kit of the Bioanalyzer 2100 system (Agilent Technologies, CA, USA).

2.4.2. Library construction and sequencing

The Illumina cDNA libraries were constructed by 3 μg RNA of each individual from two shell color (black shell color strain and golden shell color strain). Sequencing libraries were constructed using NEBNext® Ultra™ RNA Library Prep Kit for Illumina® (NEB, USA) following manufacture's protocols. Firstly, polyT oligo-attached magnetic beads were used to enrich mRNA from total RNA, and then enriched mRNA were randomly broken into fragments with fragmentation buffer. Secondly, the first-strand cDNA was synthesized using ProtoScript II Reverse Transcriptase and the second-strand cDNA was synthesized using second strand synthesis enzyme mix. Subsequently, the double-stranded cDNA was purified using Agencourt AMPure XP beads to select fragments of 150–200 bp. Thirdly, Illumina paired-end adaptors were ligated to DNA fragments after adenylation of 3' ends, and fragments were incubated with USER Enzyme (NEB) at 37°C for 15 min. Finally, the PCR was performed and PCR product was purified by AMPure XP beads. The cDNA libraries were sequenced using 150 bp paired-end reads on an Illumina NovaSeq 6000 platform.

2.4.3. Quality control, reads mapping, and transcriptome assembly

Raw sequence data was performed on the Fastp v0.20.1 package (Chen et al., 2020) to obtain clean reads which were removed adapter sequences, poly-N sequences and low-quality bases. The Q20, Q30, and GC content of the clean data were calculated. All the downstream analyses were based on the high-quality clean data.

All the RNA-seq reads were performed on the HISAT2 (Kim et al., 2015) to be mapped to the oyster genome (GenBank accession No. GCA_902806645.1). The produced SAM files were converted to BAM files and stored by SAMtools v1.10 (Li et al., 2009). The transcript assembly was performed by StringTie v2.1.2 (Pertea et al., 2015) based on the *C. gigas* genome sequence. Then, IsoformSwitchAnalyzeR was performed to extract raw read counts of all genes and each gene of fragments per kilobase per million mapped reads (FPKM) was also calculated.

2.4.4. Differential expressed gene (DEGs) identification, enrichment and pathway analysis

The DEGs between two different shell color strains were detected by the DESeq2 v1.30.1 (Wang et al., 2010). The *P* values were adjusted using the Benjamini and Hochberg method to control false discovery rate. Genes were considered as significant differentially expressed conform to the adjusted *P*-values < 0.05 and $|\log_2\text{Fold Change}| > 1$. The ClusterProfiler v4.0.2 R package was conducted to analyze Gene Ontology (GO) of DEGs (Ashburner et al., 2000). DEGs were deemed significantly enriched in GO terms with *P*-value < 0.05. Kyoto Encyclopedia of Genes and Genomes (KEGG) is a database of biological systems that provide insight into high-level functions and utilities of biological system. The statistical enrichment of DEGs in KEGG pathways was analyzed by ClusterProfiler v4.0.2 R package. KEGG pathway with corrected *P*-value < 0.05 were significantly enriched by DEGs (Kanehisa et al., 2008).

2.5. Quantitative real-time PCR validation

To validate the reliability of the transcriptome results, 5 DEGs of interest were selected to perform quantitative real-time PCR (qRT-PCR) analysis. Total RNAs were isolated from three individual samples of each color phenotype (black and golden shell color strains) and reversely transcribed to first-strand cDNA using PrimeScript™ 1st strand cDNA Synthesis kit (Takara, Japan). The qPCR was conducted on a Lightcycler® 480 real-time PCR instrument (Roche, Switzerland) using QuantiNova SYBR Green PCR kit (Qiagen, Germany). The specific primers were designed using primer premier 5.0 software (Premier Biosoft International, Palo Alto, CA) in Table S1, and its availability was detected by conventional PCR and melting curve analysis. The elongation factor 1- α (EF1- α) were used as internal control (Li et al., 2021) and relative expression were calculated using $2^{-\Delta\Delta CT}$ method (Livak and Schmittgen, 2001).

2.6. Plasmids construction, cell culture, transfection

CgTPC2 coding sequences were obtained from NCBI database and were subcloned into the pcDNA3.1(+) plasmid (Progema, USA). The plasmid constructions were based on the protocols of ClonExpress II One Step Cloning Kit (Vazyme, China). The plasmid was extracted from the DH5 α using the EndoFree Mini Plasmid Kit (OMEGA, China). The primers used in this study were provided in Table S1.

The 293T cells were cultured in DMEM (Hyclone, USA) supplemented with 10 % fetal bovine serum and 1 % 1 \times penicillin-streptomycin antibiotic solution (Hyclone, USA) with 5 % CO₂ at 37 °C. The cells were then transfected using lipofectamine 3000 (Invitrogen, USA) until the confluency up to 70–80 %. The B16F cells were cultured under the same condition, except for the medium, which was replaced with RPMI Medium Modified (Hyclone, USA).

2.7. Intracellular pH detection

Intracellular pH (pHi) was measured using the fluorescent pH-indicator BCECF-AM (Yeasen, China) following the manufacturer's protocol. BCECF-AM can penetrate the cell membrane and is cleaved by the intracellular esterases to form BCECF. The AM component is retained in the cell, emitting green fluorescence with the changes in pH. After an incubation of 30 min, the fluorescence intensity was determined using confocal microscopy with an excitation wavelength of 530 nm.

2.8. Measurements of intracellular Ca²⁺

Fluo-4 (Beyotime, China) was applied to detect intracellular Ca²⁺ concentration. The HEK293T cells and B16F cells were seeded on the confocal dishes (Corning, USA), and transfected with TPC2 over-expression plasmid. After 48 h, the culture medium was discarded and

cells were washed with PBS, and then cells were incubated with Fluo-4 staining reagent at 37 °C for 30 min. Finally, the cells were detected by fluorescence microscopy.

2.9. In vitro culture of tissues and treatment with tetrandrine

For in vitro culture experiments, the mantles were dissected from healthy one-year-old golden shell color oysters, washed with PBS (pH 7.4) three times supplemented with penicillin-streptomycin-gentamicin antibiotic solution for 30 min. Subsequently, the tissues were rinsed with culture medium containing L15 medium and M199 medium (1:1) with 10 % fetal bovine serum and 1 % 1 \times penicillin-streptomycin-gentamicin solution. The tissues were then cut into pieces and transferred to 24-well plates at 16 °C. For treatment with tetrandrine, the tetrandrine was dissolved into DMSO and added into the medium at different final concentration of 0, 5, 10, 15, and 20 μ M and maintained for 12 h. Finally, the culture medium was discarded and the cells were collected for enzyme activity detection after washing with PBS for three times.

2.10. Tyrosinase activity assays

A specific quantity of tissues was homogenized in ice bath condition, and after centrifugation, supernatant was taken for detection. Subsequently, the supernatant was mixed with a substrate solution and immediately measured for A1 at OD475nm. Afterward, it was incubated at 25 °C for 50 min and measured for A2. The tyrosinase activity was calculated as $U/g = 90.09 \times \Delta A \div W$.

3. Results

3.1. Comparison of melanin content and morphology in black and golden shell oyster

To examine the difference between black and golden phenotype in *C. gigas*, we conducted quantification, histological and ultrastructural observations to investigate the state of melanin synthesis. In contrast to the black phenotype, the histological section of golden mantle displayed light melanin pigmentation (Fig. 1A). Correspondingly, ultrastructural morphology of mantle with three different folds in black and golden phenotype showed that three folds contained melanosomes (Fig. 1B), the black phenotype contained large melanosomes, which displayed round shape, while golden phenotype melanosomes displayed fewer and irregular. Additionally, the eumelanin and pheomelanin were detected in black and golden phenotype (Fig. 1C, D). The results revealed that two color phenotypes contained two kinds pigments, including eumelanin and pheomelanin. The content of eumelanin was higher in black phenotype than in golden phenotype, whereas, the content of pheomelanin was higher in golden phenotype than in black phenotype.

3.2. Transcriptome analysis

3.2.1. Overall evaluation of transcriptome data

Six *C. gigas* cDNA libraries in black and golden shell strains were constructed and sequenced using Illumina HiSeq 2500 platform. In total, 88,879,852, 84,414,542, 84,220,654, 85,642,596, 81,837,798, and 78,124,298 clean reads were filtered from 89,504,136, 84,999,440, 84,824,798, 86,285,338, 82,593,934, and 78,600,588 raw reads, respectively, with Q20 (%) varying from 98.32 % to 98.53 % (Table S2). Among these clean reads, the Q30 in each sample was above 90 %, indicating that the RNA-seq was high quality. Compared with oyster reference genome, the gene mapping rates were over 78 % in average. After alignment, the abundances of whole genes were estimated to read count values and normalized using the TPM methods. The raw data of golden RNA-seq has been uploaded into the Sequence Read Archive (SRA) database from NCBI. The bioproject accession number was

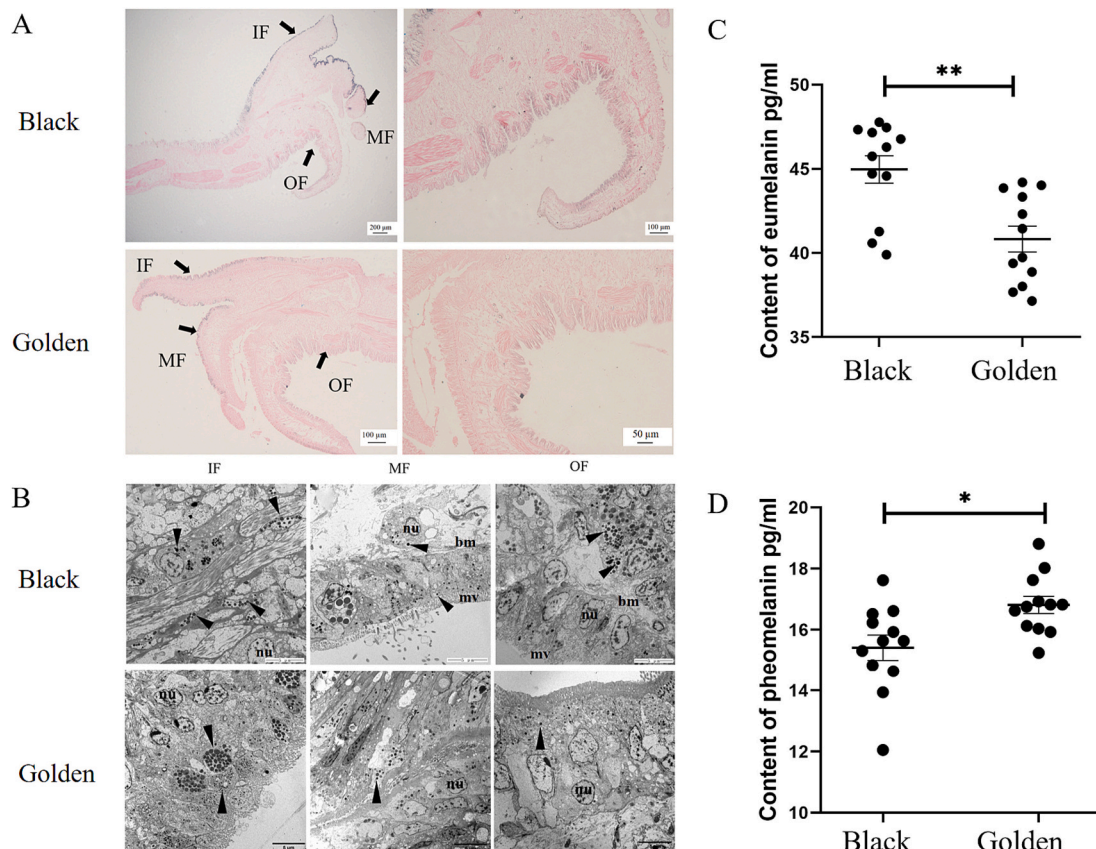


Fig. 1. Investigation of melanin distribution and composition in black and golden oysters. (A) Ferrous sulfate staining was employed to examine the presence and distribution of melanin granules in both black and golden oysters. (B) The transmission electron microphotographs depict the morphology of melanosomes in black (Images reproduced with permission from reference [Zhu et al., 2023](#)) and golden oysters. (C) The content of eumelanin and pheomelanin was detected in oysters with black and golden shell colors. Abbreviations: OF (outer fold), IF (inner fold), and MF (middle fold). * indicates statistical significant difference at $P < 0.05$.

PRJNA1067317.

3.2.2. DEG analysis

The expression level of genes is compared with six DEGs libraries based on the read counts and the differential expressed genes were detected according to corrected P -value < 0.05 and $|\log_2\text{Fold Change}| > 1$. Consequently, a total of 3525 DEGs were detected, of which 1782 and 1743 genes specially were up-regulated in B_ME and G_ME, respectively. The volcano plot was applied to intuitively present the DEGs ([Fig. 2B](#)). The heatmap determined by the analysis of the DEGs ([Fig. 2A](#)) showed that yellow and blue shadings represent higher and lower relative expression, respectively.

3.2.3. GO classification and KEGG pathway enrichment analysis of DEGs

The results demonstrated that the DEGs of *C. gigas* were most annotated in the biological process, followed by cellular component and molecular function. A total of 405, 39 and 127 GO terms were classified into biological process, cell component, and molecular function, respectively ([Fig. 2D](#)). For biological process, the major categories were biological regulation, cellular process and metabolic process. For the cellular component, the major categories were organelle and cell part. For molecular function, the major categories were mainly enriched in binding and all kinds of enzyme activity. A number of DEGs were involved in interesting categories, including lysosome organization, potassium ion transport, chloride transport, chitin binding, protein-lipid complex binding, and receptor inhibitor activity, implying that macromolecule binding and organelle organization would be contributed to pigment synthesis and transport.

DEGs in B_ME and G_ME are significantly enriched in 26 KEGG

pathways ([Fig. 2C](#)). Enrichments in PI3K-Akt signaling pathway (ko04151), MAPK signaling pathway (ko04010), Ras signaling pathway (ko04014), calcium signaling pathway (ko04020), Notch signaling pathway (ko04330), TGF-beta signaling pathway (ko04350), and glutathione metabolism (ko00480), indicating that the pigmentation of *C. gigas* is related to multi-signal transduction cooperation.

3.3. qRT-PCR validation

The accuracy of the RNA-seq was validated using qPCR. The expression level of 5 interested DEGs selected was analyzed. The specific primer for these genes were listed in Table S1. The expression of selected genes in the RNA-seq demonstrated the similar trend as that observed qPCR ([Fig. 3](#)), indicating that the results of the RNA-seq expression analysis are accurate.

3.4. TPC2 regulates Ca^{2+} release to modulate melanosome or lysosomes pH

Since TPC2 is a Ca^{2+} channel, we reasoned that the overexpression of CgTPC2 in B16F and HEK 293 T cells may be responsible for the release of Ca^{2+} from melanosome or lysosomes. In fact, overexpression of CgTPC2 in B16F and HEK 293 T cells exhibited a reduced fluorescence intensity, according to the Fluo-4 protocols, the fluorescence intensity was negatively correlated with calcium ion concentration, indicative of higher calcium ion concentration, compared with untreated group ([Figs. 4, 5](#)). In addition, TPC2-specific inhibitor tetrandrine produced a significant increase in the tyrosinase activity relative to mantle tissues of golden shell color treated with different dosages ([Fig. 6](#)).

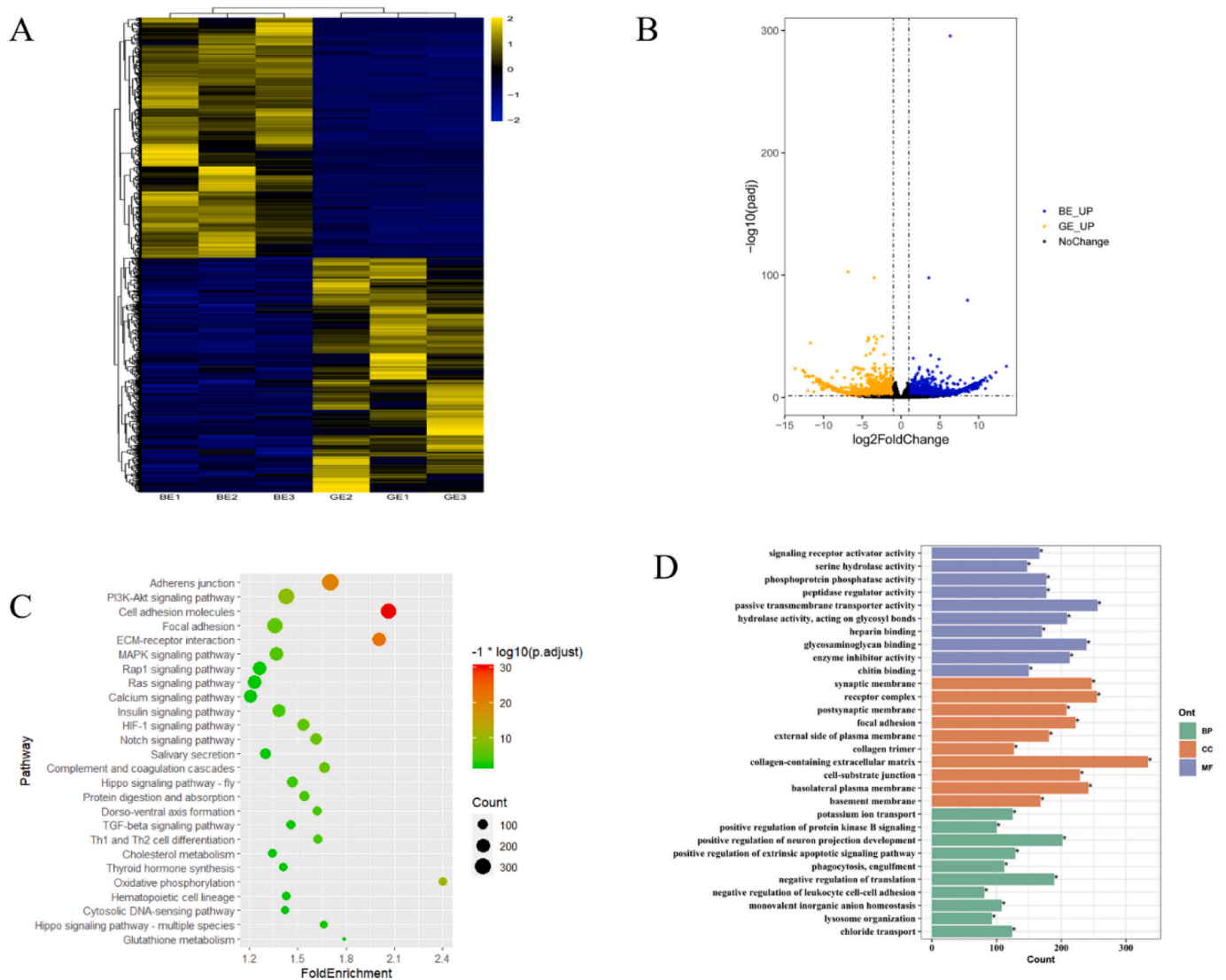


Fig. 2. Differential gene expression (DEGs) between the mantles of black and golden oysters, along with enrichment analysis. (A) The heatmap illustrates the DEGs. (B) Volcano plot depicts DEGs with orange dots and blue dots representing up-regulated genes in the golden and black shell color oysters, respectively. The black dots indicate genes with no significant differences in expression. (C) KEGG pathway enrichment analysis of the DEGs. (D) GO categorization of the DEGs. (For interpretation of the references to color in this figure legend, the reader is referred to the web version of this article.)

4. Discussion

With shell color being such a distinctive feature of bivalves, scientists and naturalists have been attracted for their visual esthetics and economic value. Studies have shown that shell color is a genetic trait (Zheng et al., 2013; Ge et al., 2015; Han and Li, 2020). Besides some model species, the molecular mechanism of pigment synthesis and transport remains vague, particular in the bivalves. The golden and black phenotype represent two distinct variations that do not naturally undergo conversion, distinguishing them from buried mollusks like the Venus clam and Manila clam, where the change in shell color is attributed to the reduction or oxidation of melanin (Wei et al., 2020). In this study, we performed RNA-seq analysis of black and golden shell color oysters to investigate vital signaling pathway and genes involved in pigmentation and putatively molecular mechanism of shell color determination in the *C. gigas*. DEGs were involved in the glutathione metabolism, calcium signaling pathway, and TGF-beta signaling pathway, which might have an impact on the pigment formation and regulation.

4.1. The distinct morphology of melanosomes between black and golden shell color oysters

Melanocytes play a crucial role in producing melanin, which contain several kinds of melanosomes, varying in size, shape, and types of melanin. Notably, two main types of melanosomes, namely eumelanosomes and pheomelanosomes, are present in variable proportions, contributing to the distinct shell coloration of black and golden oysters. The eumelanosomes, responsible for producing eumelanin, exhibit a higher electron density and tend to be smaller and more compact. In contrast, the pheomelanosomes, responsible for pheomelanin synthesis, have a lower electron density and are larger in size (D'Alba and Shawkey, 2019). One fascinating aspect is the significant morphological differences observed in the melanosomes found in the mantle of black and golden shell color oysters. The melanosomes in the mantle of black oysters tended to be regularly spherical, while those in the golden oysters were irregularly spherical and oval. It has been proposed that the irregular shape of melanosomes is due to the absence of protein scaffolds that direct the orderly deposition of melanin (Jimbow et al., 1983). Further investigation revealed interesting insights into the process of

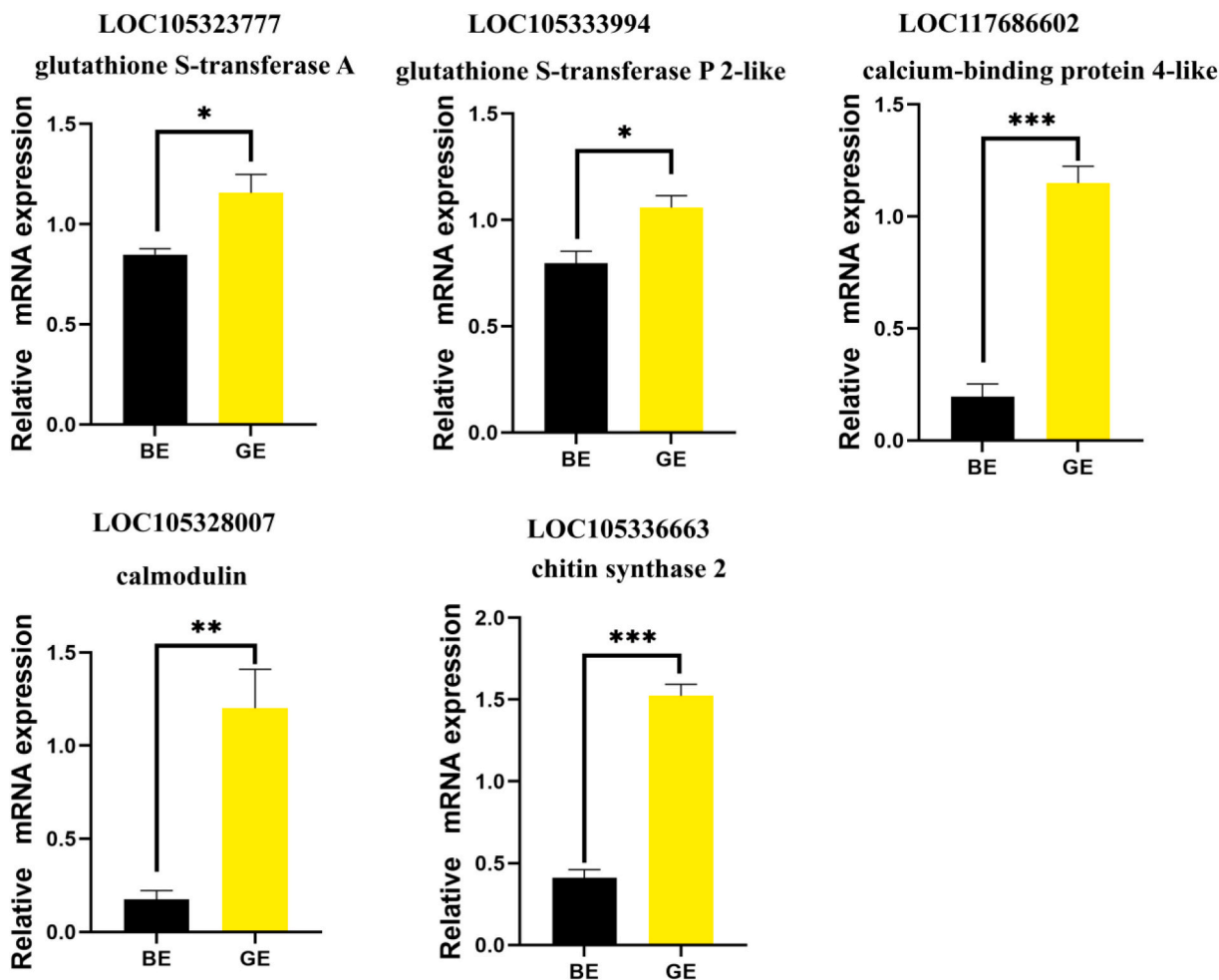


Fig. 3. Validation of RNA-Seq results using RT-qPCR.

melanin maturation and secretion in oysters. The melanin originates from the inner and middle fold, where it undergoes maturation. Ultimately, the matured melanin is secreted by the outer fold. Notably, the outer fold of the golden shell color oysters contained relatively fewer matured melanosomes compared to black oysters, which could potentially explain their unique irregular melanosome shape and, consequently, their distinctive golden shell coloration.

Significant differences are evident in the development of eumelanosomes and pheomelanosomes, primarily arising from variations in the types and ratios of melanin they contain. The balance between eumelanin and pheomelanin is intricately linked to the presence and activity of tyrosinase, responsible for converting L-tyrosine into L-dopaquinone (DQ) (Ito and Wakamatsu, 2011). During the initial stage of melanogenesis, the availability of L-cysteine (Cys) within melanosomes plays a crucial role. DQ interacts with Cys, leading to the production of pheomelanin (D'Alba and Shawkey, 2019). The transition from eumelanin to pheomelanin production can be induced by changes in the pH environment within melanosomes. Eumelanogenesis typically occurs around neutral pH levels, but under acidic conditions, pheomelanin production accelerates, even suppressing eumelanin synthesis altogether (Ito et al., 2013; Wakamatsu et al., 2017). This phenomenon underscores the pivotal role of pH regulation in determining the types of melanin synthesized (Wakamatsu et al., 2017).

4.2. The golden shell trait in *C. gigas* might be affected by glutathione metabolism

The glutathione system, a vital component of melanogenesis,

comprises key elements such as glutathione (GSH), glutathione disulphide (GSSG), glutamate cysteine ligase (GCL), glutathione synthetase (GSS), GPx, GR and NADPH. Notably, GSH not only functions as an antioxidant by scavenging free radicals but also actively participates in pheomelanin formation (Lu et al., 2021). The cystine/glutamate antiporter (xCT) emerges as pivotal enzyme in modulating the glutathione system, swiftly converting to cysteine, a crucial ingredient for GSH synthesis. By conjugating with dopaquinone, GSH and cysteine form pheomelanin intermediates, switching eumelanin to pheomelanin (Lu et al., 2021). Notably, experiments with xCT-transgenic sheep, generated through a testicular injection transgenic approach, exhibited patches of brown/yellow coat, highlighting the role of xCT in promoting pheomelanin production (He et al., 2012). In *C. gigas*, xCT RNAi experiment presented less brown-granules in the silencing group of orange shell color (Li et al., 2023). These findings shed light on the function of xCT in melanogenesis and propose that further research should be taken to determine how it affects pheomelanin formation.

Another key player in the glutathione system is Glutathione S-transferase (GST). qRT-PCR analysis revealed that GST-related genes exhibit higher expression in the golden shell color compared to the black shell color, suggesting the likely involvement of GST in pheomelanin formation. Considering the correlation between melanogenesis and intracellular redox state, primarily controlled by thiol-based antioxidants, GST in the GSH system likely plays a key role in regulating pigmentation and responding to oxidative stress associated with melanogenesis. It is worth noting that the production of eumelanin requires low levels of GSH, whereas the production of pheomelanin requires high levels of GSH (Teerikorpi et al., 2019), which serve as the primary

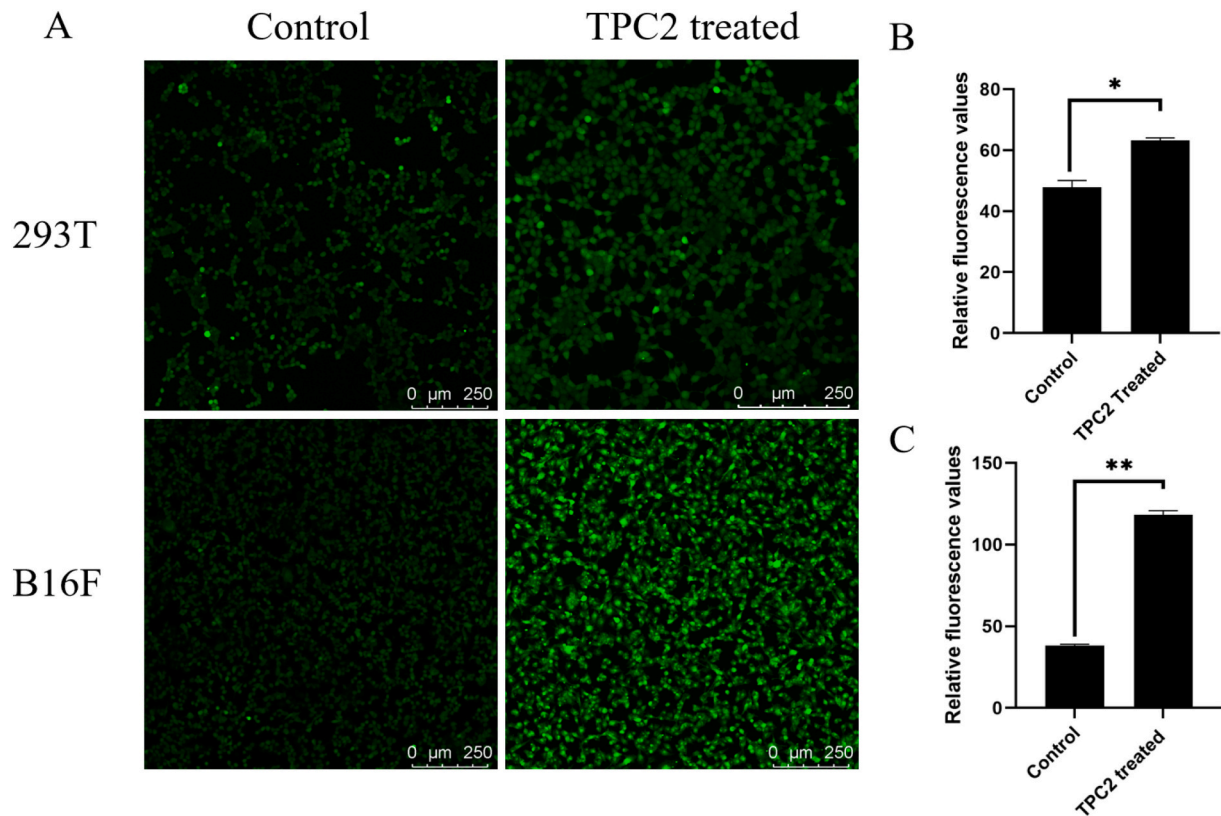


Fig. 4. Confocal fluorescence microscopy depicting the Ca^{2+} concentration in HEK293T and B16F cells expressing TPC2-pcDNA3.1 (A). The fluorescence intensity is directly correlates with Ca^{2+} concentration. Intensity ratios were determined for both HEK 293 T cells and B16F cells (B, C).

cysteine reservoir. Cysteine is able to react with dopaquinone, contributing to the formation of pheomelanin in melanosomes (Galván et al., 2012). GST acts as a catalyst in the conjugation process, ensuring the efficient synthesis of pheomelanin (Lu et al., 2021).

4.3. Genes involved in calcium signaling regulation might influence melanogenesis in the mantle edge of the *C. gigas*

In premelanosomes, Ca^{2+} plays an indispensable role in the activity of furin-like protease, facilitating the cleavage of PMEL and contributing to premelanosomal fibril formation (D'Alba and Shawkey, 2019). Beyond its involvement in melanogenesis, Ca^{2+} also plays a crucial role in signaling responses between melanosomes and melanocytes. Functioning as an essential second messenger, Ca^{2+} actively regulates melanogenesis (Schallreuter et al., 2008). Transport of cytosolic Ca^{2+} into melanosomes enhances tyrosinase activity, initiates melanin transfer and regulate organelle interaction (Zhang et al., 2022). Interestingly, calcium exhibits a high affinity for binding to melanin, effectively controlling the redox state of melanocytes and offering protection against oxidative damage by reactive oxygen species (ROS) (Hoogduijn et al., 2004). This intricate relationship underscores the significance of calcium signaling in melanogenesis. Moreover, previous research has emphasized the role of various metal elements, including Ca, copper (Cu), iron (Fe), and zinc (Zn), in the production of intermediates involved in eumelanin and pheomelanin synthesis. These metal elements serve as common enzyme cofactor and essential components (Zduniak et al., 2014), influencing the delicate balance between eumelanin and pheomelanin synthesis. Variations in metal concentrations are intricately linked to the ratio of eumelanin and pheomelanin, further highlighting the complex regulatory mechanisms governing melanogenesis.

Calmodulin (CaM), a well-established calcium sensor, plays a central role in orchestrating calcium-dependent signaling pathway (Yang and

Tsai, 2021). Its remarkably flexible structure allows for interactions with diverse proteins, precisely adjusting its conformation upon calcium binding (Yang and Tsai, 2021). The qRT-PCR analysis demonstrated higher expression levels of calcium-binding protein and calmodulin in golden oyster compared to black oysters, suggesting an increased influx of Ca^{2+} . The upregulation of calmodulin further supports the increased influx of Ca^{2+} (Ahmed et al., 2021), subsequently resulting in an increase in tyrosinase activity (Buffey et al., 1993). As previously mentioned, melanin production is directly proportional to DQ formation, which, in turn, depends on tyrosinase activity. Therefore, the ration of eumelanin to pheomelanin is determined by both tyrosinase activity and cysteine availability in melanosomes (Land et al., 2003). Additionally, it is worth noting that pheomelanogenesis is affected more by a decrease in tyrosinase activity than eumelanogenesis (Barsh, 1996; Ollmann et al., 1998). Calmodulin and other related proteins are related to tyrosinase activity, further influencing DQ's binding with cysteine for pheomelanin synthesis.

4.4. Melanosomal pH regulation may contribute to golden shell color pigmentation

Melanosomal pH plays a critical role in controlling both eumelanin and pheomelanin. At low pH conditions, the activity of tyrosinase is suppressed, resulting in an increase in pheomelanogenesis (Wakamatsu et al., 2021). Maintaining the intricate regulation of melanosomal pH involves the concerted actions of proton pumps, ion channels, and transporters, which finely control the establishment and maintenance of electrochemical gradients (Wakamatsu et al., 2021). Among these regulators, Two-pore channel 2 (TPC2) stands out as a crucial ion transport protein, functioning as a ligand-gated cation channel independently of voltage changes (Wakamatsu et al., 2021). Reportedly, TPC2 deficiency impacts both melanosomal pH and size, as well as melanin synthesis (Ambrosio et al., 2016). Additionally, TPC2 contributes to pH

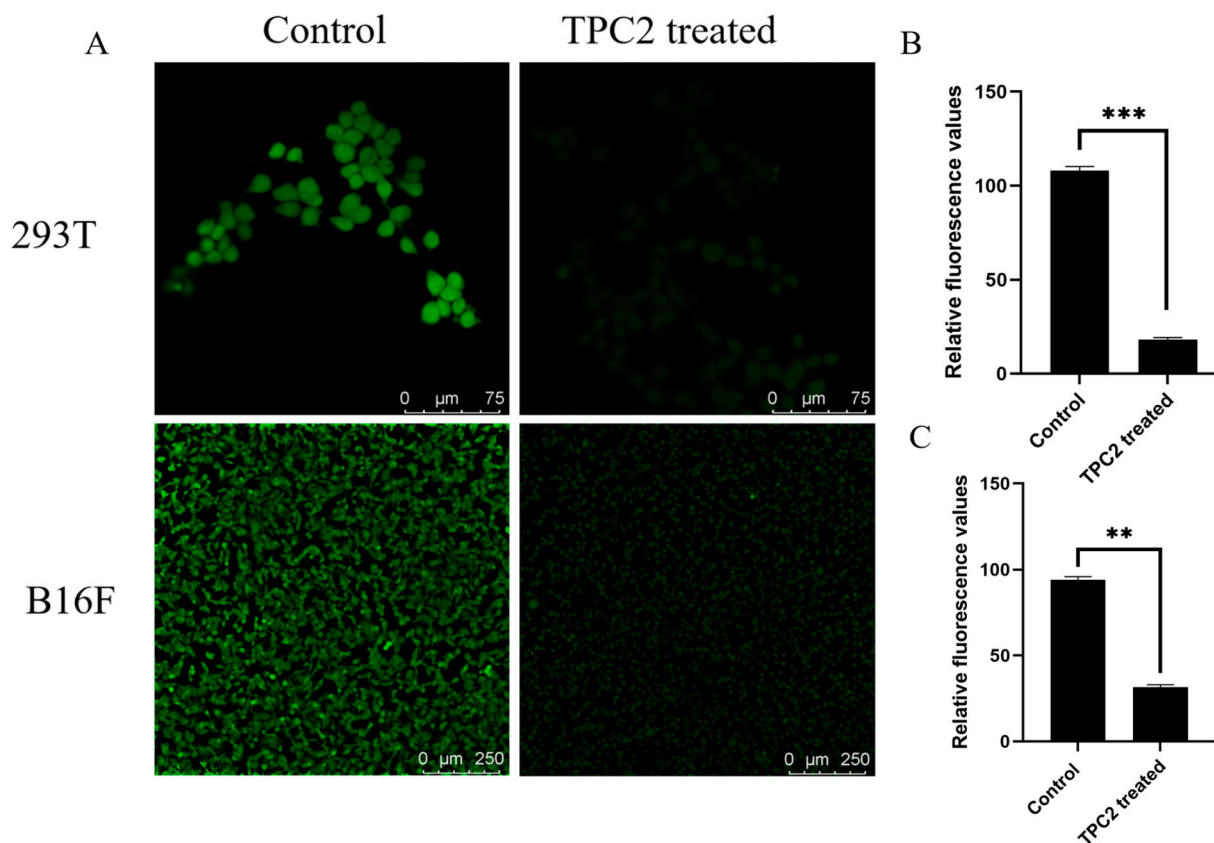


Fig. 5. Confocal fluorescence microscopy images illustrating intracellular pH in HEK293T and B16F cells expressing TPC2-pcDNA3.1 (A). The fluorescence intensity varies inversely with intracellular pH. Intensity ratios were calculated for both HEK 293T cells and B16F cells (B, C).

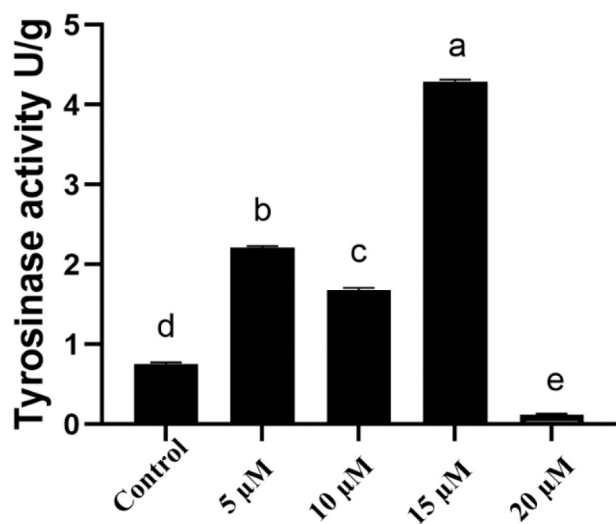


Fig. 6. Assessment of tyrosinase activity in mantle tissues following treatment with various dosages of tetrandrine. Data is presented as the mean \pm SD (n = 3). The different lowercase represents statistically significant difference ($P < 0.05$).

maintenance by serving as a negative regulator, influencing both melanin production and pH neutralization (Ambrosio et al., 2016; Bellono et al., 2016). Based on the presented results, a significant increase in tyrosinase activity was observed following treatment with the TPC2-specific inhibitor tetrandrine in the mantle tissues of golden shell color oysters. This finding suggests a potential overexpression of TPC2 in the golden shell color oysters, which may modulate melanosomal pH and

subsequently influence tyrosinase activity, resulting in reduced eumelanin synthesis. Moreover, we observed a reduction in intracellular pH and a concurrent increase in Ca^{2+} concentration following CgTPC2 overexpression in both 293T and B16F cells. These findings provided compelling evidence of TPC2 role in intracellular pH homeostasis and Ca^{2+} dynamics, with potential implications for various cellular processes, including melanogenesis. Consistent with our results, prior studies have emphasized that the impact of Ca^{2+} on melanosomal pH regulation constitutes a complex yet intriguing aspect of cellular physiology and pigmentation mechanisms, warranting further investigation.

5. Conclusion

In this study, we conducted a comparative analysis of the mantle transcriptome between black and golden shell strains of Pacific oysters. Our investigations revealed several crucial regulatory pathways and genes associated with pheomelanogenesis, including glutathione metabolism, the calcium signaling pathway, calmodulin, and TPC2. With integration of RNA-seq and functional assays, these combined findings emphasize the pivotal role of CgTPC2 in the regulation of cellular pH and Ca^{2+} concentration. This insight provided valuable information regarding the potential implications of CgTPC2 in melanogenesis and pigmentation processes.

Supplementary data to this article can be found online at <https://doi.org/10.1016/j.cbd.2024.101197>.

CRediT authorship contribution statement

Yue Min: Writing – review & editing, Writing – original draft, Data curation. **Qi Li:** Writing – review & editing, Supervision, Resources, Project administration, Funding acquisition. **Hong Yu:** Methodology. **Lingfeng Kong:** Resources, Data curation. **Shikai Liu:** Software, Formal

analysis, Data curation, Conceptualization.

Declaration of competing interest

The authors declare that they have no known competing financial interests or personal relationships that could have appeared to influence the work reported in this paper.

Data availability

The data that has been used is confidential.

Acknowledgements

This research was supported by grants from National Natural Science Foundation of China (32373115), Shandong Province (2021ZLGX03 and 2022LZGCQY010), and the Agriculture Research System of China Project (CARS-49).

References

- Ahmed, M.B., Islam, S.U., Lee, Y.S., 2021. PRP4 promotes skin cancer by inhibiting production of melanin, blocking influx of extracellular calcium, and remodeling cell actin cytoskeleton. *Int. J. Mol. Sci.* 22, 6992.
- Ambrosio, A.L., Boyle, J.A., Aradi, A.E., Christian, K.A., Di Pietro, S.M., 2016. TPC2 controls pigmentation by regulating melanosome pH and size. *Proc. Natl. Acad. Sci. U. S. A.* 113, 5622–5627.
- Ashburner, M., Ball, C.A., Blake, J.A., Botstein, D., Butler, H., Cherry, J.M., Davis, A.P., Dolinski, K., Dwight, S.S., Eppig, J.T., Harris, M.A., Hill, D.P., Issel-Tarver, L., Kasarskis, A., Lewis, S., Matese, J.C., Richardson, J.E., Ringwald, M., Rubin, G.M., Sherlock, G., Gene Ontology, C., 2000. Gene Ontology: tool for the unification of biology. *Nat. Genet.* 25, 25–29.
- Barsh, G.S., 1996. The genetics of pigmentation: from fancy genes to complex traits. *Trends Genet.* 12, 299–305.
- Bellono, N., Escobar, I., Oancea, E., 2016. A melanosomal two-pore sodium channel regulates pigmentation. *Sci. Rep.* 6, 26570.
- Brake, J., Evans, F., Langdon, C., 2004. Evidence for genetic control of pigmentation of shell and mantle edge in selected families of Pacific oysters, *Crassostrea gigas*. *Aquaculture* 229, 89–98.
- Buffey, J.A., Edgecombe, M., Mac Neil, S., 1993. Calcium plays a complex role in the regulation of melanogenesis in murine B16 melanoma cells. *Pigment Cell Res.* 6, 385–393.
- Caro, T., Mallarino, R., 2020. Coloration in mammals. *Trends Ecol. Evol.* 35, 357–366.
- Chen, M., Liu, B., Ma, B., Liu, G.L., Cao, W.A., Liu, X., Yan, X.J., Yang, B., Wang, C.D., 2020. Selection of a carotenoid-rich scallop strain, QN Orange, from the inter-specific hybrids between the bay scallop and the Peruvian scallop. *Aquaculture* 528.
- D'Alba, L., Shawkey, M.D., 2019. Melanosomes: biogenesis, properties, and evolution of an ancient organelle. *Physiol. Rev.* 99, 1–19.
- Galván, I., Ghanem, G., Möller, A.P., 2012. Has removal of excess cysteine led to the evolution of pheomelanin? Pheomelanogenesis as an excretory mechanism for cysteine. *BioEssays* 34, 565–568.
- Ge, J.L., Li, Q., Yu, H., Kong, L.F., 2015. Mendelian inheritance of golden shell color in the Pacific oyster *Crassostrea gigas*. *Aquaculture* 441, 21–24.
- Han, Z.Q., Li, Q., 2020. Mendelian inheritance of orange shell color in the Pacific oyster *Crassostrea gigas*. *Aquaculture* 516.
- Harpaz, S., Padowicz, D., 2007. Color enhancement in the ornamental dwarf cichlid *Microgeophagus ramirezi* by addition of plant carotenoids to the fish diet. *Isr. J. Aquac.* 59, 195–200.
- He, X., Li, H., Zhou, Z., Zhao, Z., Li, W., 2012. Production of brown/yellow patches in the SLC7A11 transgenic sheep via testicular injection of transgene. *J. Genet. Genomics* 39, 281–285.
- Hoogduijn, M.J., Cemeli, E., Ross, K., Anderson, D., Thody, A.J., Wood, J.M., 2004. Melanin protects melanocytes and keratinocytes against H₂O₂-induced DNA strand breaks through its ability to bind Ca²⁺. *Exp. Cell Res.* 294, 60–67.
- Hubbard, J.K., Uy, J.A., Hauber, M.E., Hoekstra, H.E., Safran, R.J., 2010. Vertebrate pigmentation: from underlying genes to adaptive function. *Trends Genet.* 26, 231–239.
- Ito, S., Wakamatsu, K., 2011. Human hair melanins: what we have learned and have not learned from mouse coat color pigmentation. *Pigment Cell Melanoma Res.* 24, 63–74.
- Ito, S., Suzuki, N., Takebayashi, S., Commo, S., Wakamatsu, K., 2013. Neutral pH and copper ions promote eumelanogenesis after the dopachrome stage. *Pigment Cell Melanoma Res.* 26, 817–825.
- Jimbow, K., Ishida, O., Ito, S., Hori, Y., Witkop Jr., C.J., King, R.A., 1983. Combined chemical and electron microscopic studies of pheomelanosomes in human red hair. *J. Invest. Dermatol.* 81, 506–511.
- Kanehisa, M., Araki, M., Goto, S., Hattori, M., Hirakawa, M., Itoh, M., Katayama, T., Kawashima, S., Okuda, S., Tokimatsu, T., Yamanishi, Y., 2008. KEGG for linking genomes to life and the environment. *Nucleic Acids Res.* 36, D480–D484.
- Kang, J.H., Kang, H.S., Lee, J.M., An, C.M., Kim, S.Y., Lee, Y.M., Kim, J.J., 2013. Characterizations of Shell and mantle edge pigmentation of a Pacific oyster, *Crassostrea gigas*, in Korean Peninsula. *Asian-Australas. J. Anim. Sci.* 26, 1659–1664.
- Kim, D., Landmead, B., Salzberg, S.L., 2015. HISAT: a fast spliced aligner with low memory requirements. *Nat. Methods* 12, 357–360.
- Kobayashi, T., Kawahara, I., Hasekura, O., Kijima, A., 2004. Genetic control of bluish shell color variation in the Pacific abalone, *Haliotis discus hannai*. *J. Shellfish Res.* 23, 1153–1156.
- Ky, C.L., Nakasai, S., Pommier, S., Sham Koua, M., Devaux, D., 2016. The Mendelian inheritance of rare flesh and shell colour variants in the black-lipped pearl oyster (*Pinctada margaritifera*). *Anim. Genet.* 47, 610–614.
- Lai, X., Wichers, H.J., Soler-Lopez, M., Dijkstra, B.W., 2018. Structure and function of human tyrosinase and tyrosinase-related proteins. *Chemistry* 24, 47–55.
- Land, E.J., Ito, S., Wakamatsu, K., Riley, P.A., 2003. Rate constants for the first two chemical steps of eumelanogenesis. *Pigment Cell Res.* 16, 487–493.
- Li, H., Handsaker, B., Wysoker, A., Fennell, T., Ruan, J., Homer, N., Marth, G., Abecasis, G., Durbin, R., 1000 Genome Project Data Processing Subgroup, 2009. The sequence alignment/map format and SAMtools. *Bioinformatics* 25, 2078–2079.
- Li, H., Yu, H., Li, Q., 2021. Striated myosin heavy chain gene is a crucial regulator of larval myogenesis in the Pacific oyster *Crassostrea gigas*. *Int. J. Biol. Macromol.* 179, 388–397.
- Li, Z., Hu, B., Du, L., Hou, C., Li, Q., 2023. Involvement of B-aat1 and Cbs in regulating mantle pigmentation in the Pacific oyster (*Crassostrea gigas*). *Mol. Biol. Rep.* 50, 377–387.
- Liu, X., Wu, F., Zhao, H., Zhang, G., Guo, X., 2009. A novel shell color variant of the Pacific abalone *Haliotis discus hannai* Ino subject to genetic control and dietary influence. *J. Shellfish Res.* 28, 419–424.
- Livak, K.J., Schmittgen, T.D., 2001. Analysis of relative gene expression data using real-time quantitative PCR and the 2^{-ΔΔC_T} method. *Methods* 25, 402–408.
- Lu, Y., Tonissen, K.F., Di Trapani, G., 2021. Modulating skin colour: role of the thioredoxin and glutathione systems in regulating melanogenesis. *Biosci. Rep.* 41, BSR20210427.
- Luttikhoven, P.C., Drent, J., 2008. Inheritance of predominantly hidden shell colours in *Macoma balthica* (L.) (Bivalvia:tellinidae). *J. Moll. Stud.* 74, 363–371.
- Ollmann, M.M., Lamoreux, M.L., Wilson, B.D., Barsh, G.S., 1998. Interaction of agouti protein with the melanocortin-1 receptor in vitro and in vivo. *Genes Dev.* 12, 316–330.
- Pavan, W.J., Sturm, R.A., 2019. The genetics of human skin and hair pigmentation. *Annu. Rev. Genomics Hum. Genet.* 20, 41–72.
- Pertea, M., Pertea, G.M., Antonescu, C.M., Chang, T.C., Mendell, J.T., Salzberg, S.L., 2015. StringTie enables improved reconstruction of a transcriptome from RNA-seq reads. *Nat. Biotechnol.* 33, 290–295.
- Raposo, G., Marks, M.S., 2007. Melanosomes—dark organelles enlighten endosomal membrane transport. *Nat. Rev. Mol. Cell Biol.* 8, 786–797.
- Schallreuter, K.U., Kothari, S., Chavan, B., Spencer, J.D., 2008. Regulation of melanogenesis—controversies and new concepts. *Exp. Dermatol.* 17, 395–404.
- Solano, F., 2018. On the metal cofactor in the tyrosinase family. *Int. J. Mol. Sci.* 19, 633.
- Sun, D., Qi, X., Wen, H., Li, C., Li, J., Chen, J., Tao, Z., Zhu, M., Zhang, X., Li, Y., 2023. The genetic basis and potential molecular mechanism of yellow-albino northern snakehead (*Channa argus*). *Open Biol.* 13, 220235.
- Teerikorpi, P.E., Staffer, J., Ilmonen, P., Calhim, S., Schuett, W., Laaksonen, T., 2019. Elevated oxidative stress in pied flycatcher nestlings of eumelanin foster fathers under low rearing temperatures. *J. Exp. Biol.* 222, jeb195909.
- Wakamatsu, K., Nagao, A., Watanabe, M., Nakao, K., Ito, S., 2017. Pheomelanogenesis is promoted at a weakly acidic pH. *Pigment Cell Melanoma Res.* 30, 372–377.
- Wakamatsu, K., Zippin, J.H., Ito, S., 2021. Chemical and biochemical control of skin pigmentation with special emphasis on mixed melanogenesis. *Pigment Cell Melanoma Res.* 34, 730–747.
- Wang, L.K., Feng, Z.X., Wang, X., Wang, X.W., Zhang, X.G., 2010. DEGseq: an R package for identifying differentially expressed genes from RNA-seq data. *Bioinformatics* 26, 136–138.
- Wei, M., Ge, H., Shao, C., Yan, X., Nie, H., Duan, H., Liao, X., Zhang, M., Chen, Y., Zhang, D., Dong, Z., 2020. Chromosome-level clam genome helps elucidate the molecular basis of adaptation to a buried lifestyle. *iScience* 23, 101148.
- Wen, H.B., Gu, R.B., Cao, Z.M., Zhou, X., Nie, Z.J., Ge, X., 2013. Variation of color and ray pattern in juvenile shells in hatchery-produced freshwater triangle pearl mussels, *Hyriopsis cumingii*, in China. *J. World Aquacult. Soc.* 44, 154–160.
- Winkler, F.M., Estevez, B.F., Jollan, L.B., Garrido, J.P., 2001. Inheritance of the general shell color in the scallop *Argopecten purpuratus* (Bivalvia: Pectinidae). *J. Hered.* 92, 521–525.
- Xu, C.X., Li, Q., Yu, H., Liu, S.K., Kong, L.F., Chong, J.D., 2019. Inheritance of shell pigmentation in Pacific oyster *Crassostrea gigas*. *Aquaculture* 512, 734249.
- Xu, L., Li, Q., Yu, H., Kong, L.F., 2017. Estimates of heritability for growth and Shell color traits and their genetic correlations in the black shell strain of Pacific oyster *Crassostrea gigas*. *Marine Biotechnol.* 19, 421–429.
- Yang, C.F., Tsai, W.C., 2021. Calmodulin: the switch button of calcium signaling. *Tzu Chi Med. J.* 34, 15–22.
- Yue, X., Nie, Q., Xiao, G.Q., Liu, B.Z., 2015. Transcriptome analysis of shell color-related genes in the clam *Meretrix meretrix*. *Marine Biotechnol.* 17, 364–374.
- Zduniak, P., Surmacki, A., Erciyas-Yavuz, K., Chudzińska, M., Barańkiewicz, D., 2014. Are there different requirements for trace elements in eumelanin- and pheomelanin-based color production? A case study of two passerine species. *Comp. Biochem. Physiol. A: Mol. Integr. Physiol.* 175, 96–101.

Zhang, H., Chen, Z., Zhang, A., Gupte, A.A., Hamilton, D.J., 2022. The role of calcium signaling in melanoma. *Int. J. Mol. Sci.* 23, 1010.

Zheng, H.P., Zhang, T., Sun, Z.W., Liu, W.H., Liu, H.L., 2013. Inheritance of shell colours in the noble scallop *Chlamys nobilis* (bivalve: Pectinidae). *Aquacult. Res.* 44, 1229–1235.

Zhu, Y.J., Li, Q., Yu, H., Liu, S.K., 2023. Pigment distribution and secretion in the mantle of the Pacific oyster (*Crassostrea gigas*). *J. Ocean Univ. China* 22, 813–820.